Spatial composition of the diahaline overturning circulation in a fjord–type, non–tidal estuarine system

Erika Henell[1], Hans Burchard[1], Ulf Gräwe[1], and Knut Klingbeil[1]

[1]Leibniz Institute for Baltic Sea Research Warnemünde (IOW), Rostock, Germany

Key Points:

- The local diahaline mixing per salinity class is associated with the overturning circulation
- The spurious numerical contribution to the total diahaline exchange flow is around 50% over a large range of salinity classes
- Hot spots for diahaline exchange flow are located at sloping topography and where isohalines encounter surface (outflow) or bottom (inflow)

Corresponding author: Erika Henell, `erika.henell@io-warnemuende.de`

Abstract

In this study we present new insights into the overturning circulation in non-tidal, fjord-type estuarine systems associated with diahaline mixing. As a realistic example we analyze two years of numerical model results for the Baltic Sea, a brackish semi-enclosed marginal sea, characterized by strong freshwater surplus. An isohaline water mass transformation framework is applied to quantify and decompose the diahaline exchange flow. Time-averaged effective vertical diahaline velocity is directly calculated from the divergence of the transports below the respective isohaline surface. It is furthermore indirectly estimated from the gradient of local mixing per salinity class with respect to salinity. Under the assumption of negligible horizontal salt transports both estimates should be identical. Our analysis shows a high correlation between the spatial patterns of the two estimates for the diahaline exchange flow. Two dominant types of diahaline exchange flow are analyzed. First of all there is a large scale overturning circulation with inflow at places where the isohaline surface is close to the bottom and with outflow at places where the isohaline is surfacing. Secondly, there is the well-known small-scale overturning circulation localized inside the bottom boundary layer over sloping bathymetry, associated with boundary mixing. Both types of circulation are visualized across selected vertical transects in physical and in salinity space. One major result is that about 50% of the diahaline exchange flow patterns are generated by numerical mixing caused by the truncation error of the advection scheme, despite the fact that an anti-diffusive advection scheme and vertically-adaptive coordinates are used.

Plain Language Summary

We study the major circulation in estuaries controlled by mixing of water masses. A theoretical framework is applied that replaces depth with salinity, since the latter is descriptive of the circulating water masses. The circulation is described from a point of view where the flow crosses areas of constant salinity. This is the diahaline circulation. The framework breaks down the circulation into smaller chunks, and allows us to deduce how the circulating flow depends on mixing. An application of this theory in a two-year long computer simulation of the large and non-tidal estuary of the Baltic Sea is demonstrated. Two dominant types of diahaline circulation are analyzed. The first is a large-scale circulation where water masses flow into the estuary where the areas of constant salinity touch the bottom, and out where they encounter the surface. The second is a small-scale circulation close to the bottom where the ocean bathymetry is sloping, and is controlled by boundary mixing. Both types of diahaline circulation are visualized in this study. One major result is that around 50% of the circulation is generated by unwanted spurious mixing, which is created by the computer simulation and does not exist in reality.

1 Introduction

Estuaries can be termed as "mixing machines", as Wang et al. (2017) put it, where saline ocean water is mixed with freshwater from rivers and precipitation, to form brackish water with intermediate salinity. Due to salinity being an ideal tracer for the different water masses in estuaries, an isohaline framework (a space where the vertical coordinate is replaced by salinity) is well suited for the analysis of the estuarine mixing and the resulting exchange flow.

The isohaline framework builds on the early Knudsen theorem (Knudsen, 1900), which quantifies the exchange flow in terms of bulk values for the inflowing and outflowing volume fluxes, as well as representative salinities. This initial theory was extended several decades later by Walin (1977), and even later by MacCready (2011). In these works, the stratification and flow are permitted to be continuous and to vary with space and time. The following step is essential in these theories: the time–averaged volume trans-

port per salinity class $q(S)$ is calculated by binning and averaging the transport in salinity classes. A balance must hold inside the estuary between (i) the net inflow of volume and salt with salinities above the salinity of a reference isohaline at an estuarine control section, and (ii) respectively the volume transports or advective and diffusive salt transports across the isohaline surface with the reference salinity (Walin, 1977). Furthermore, the inflow (outflow) volume transport, Q_{in} (Q_{out}), is obtained through integration of $q(S)$ in salinity space for inflows (outflows) according to MacCready (2011). This theoretical framework was termed the Total Exchange Flow (TEF) analysis framework (MacCready, 2011). Various studies have adopted the TEF analysis framework to investigate diverse types of estuarine systems (Chen et al., 2012; Sutherland et al., 2011; Gräwe et al., 2016; Purkiani et al., 2016; Burchard et al., 2018, among others) . Analyses of dynamics in estuaries and river plumes using isohaline surfaces as reference have been carried out by MacCready and Geyer (2001), MacCready et al. (2002), and Hetland (2005). The TEF analysis, however, is limited to the study of transports at a single transect in space. The spatial information remains unknown in this analysis, so does the knowledge about diahaline fluxes.

Subsequent research has taken the TEF theory further by linking it to different quantities, notably estuarine mixing. In these various research endeavours, the following suggestion by Burchard and Rennau (2008) has proven to be key: quantify mixing as the (local) destruction of salinity variance per unit volume χ^S. The integrated mixing within a given volume can then be quantified as $\mathbb{M} = \int \chi \, dV$. Moreover, this method for the analysis of mixing, renders it possible in numerical models to accurately separate the mixing into physical and numerical contributions (Burchard & Rennau, 2008; Klingbeil et al., 2014). The physical contribution is associated with the explicit diffusion from turbulence parameterizations. The numerical contribution is associated with the implicit diffusion due to the truncation errors of advection schemes in a numerical model.

The TEF was linked to the entrainment and diffusive salt flux, which in turn disclosed a relationship between mixing and TEF (Wang et al., 2017). The latter relationship was further developed in MacCready et al. (2018), where it was shown that the long-term time-averaged mixing in an estuary behind a fixed transect is approximately given by the relation $\mathbb{M} \approx S_{in} S_{out} Q_r$, where S_{in} (S_{out}) is the inflow (outflow) salinity at the boundary transect, and Q_r describes the volume flux discharged by the river. Exact mixing formulas allowing for continuous and time–dependent exchange flow was derived in Burchard et al. (2019). Furthermore, a universal law of estuarine mixing was derived in Burchard (2020). These approaches resulted in the relation $\mathbb{M}(S) = S^2 Q_r$ for the long–term averaged mixing inside an estuarine volume bounded by the isohaline of salinity S. A visual distinction between the different mixing relations described here is compiled in Fig. 1. The universal law can also be formulated as $\mathbb{m}(S) = \partial \mathbb{M}(S)/\partial S = 2S Q_r$, with $\mathbb{m}(S)$ being the salinity variance dissipation per unit salinity. In the following $\mathbb{m}$ will be referred to as mixing per salinity class (per infinitesimal salinity bin).

The isohaline framework also offers to diagnose diahaline fluxes that give new insights, as was done in Wang et al. (2017). They showed the overturning circulation in salinity space along the Hudson River (respectively their Fig. 5 b, c). The exchange flow was observed to drive the saline water landward, and the brackish water oceanward. Mixing was seen to show maxima around the interface between the inflowing and outflowing water. The diahaline transport (referred to as entrainment there) was in upward direction (towards lower salinity classes) below the interface and in downward direction (towards higher salinity classes) above. Similarly, the diahaline exchange flow was studied for the Pearl River Estuary (Li et al., 2022). They find that the diahaline exchange flow shows a classical exchange flow consisting of inflow in the deeper and outflow in the shallower water layers. The magnitude of the inflowing and outflowing diahaline transport is found to increase with salinity, while the net diahaline transport stays constant, amounting to Q_r after long enough temporal averaging. The progress made by Li et al.

transect

$\mathbb{M} \approx S_{\text{in}} S_{\text{out}} Q_{\text{r}}$ (MacCready et al., 2018)

intermediate case when isohaline
is partly outside model domain
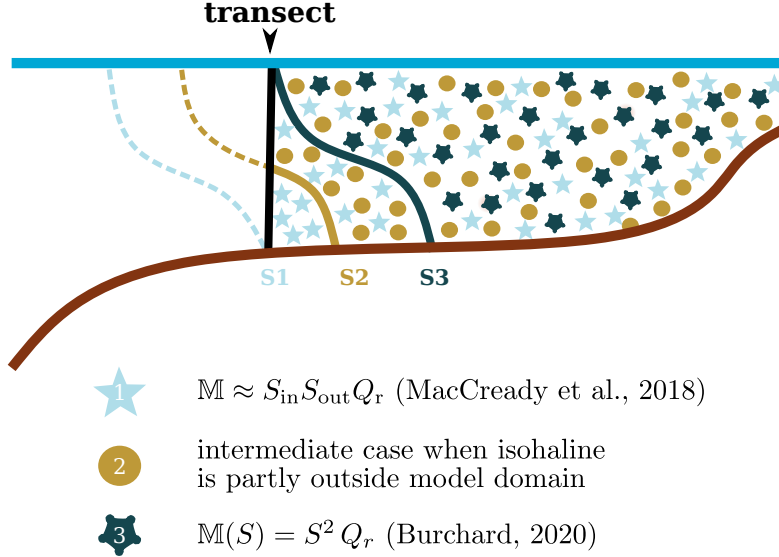
$\mathbb{M}(S) = S^2 Q_r$ (Burchard, 2020)

Figure 1. Sketch showing the differences in which areas the mixing formulas encompass. In mixing formula 1 (MacCready et al., 2018) the estuarine volume is bounded by the transect. In mixing formula 3 (Burchard, 2020) the volume of interest is bounded entirely by an isohaline (S3). In regional models, the intermediate scenario is often encountered, where the bounding isohaline (S2) is partially inside, partially outside of the model domain. Then the volume of interest is partly bounded by the isohaline and the transect.

(2022) is that horizontal maps were shown of the diahaline velocity and the *local* mixing per salinity class (their Fig. 6). They found that high diahaline velocity correlated with strong mixing. Along the same line of research are the horizontal maps of the diapycnal velocity to study the spatial composition of the Atlantic Meridional Overturning Circulation in Sidorenko et al. (2020, their Figs. 5 and B4). In studies of numerical diapycnal mixing, diapycnal velocity maps of the Southern Ocean and the World Ocean were presented in, respectively, Lee et al. (2002, their Fig. 7) and Megann (2018, his Fig. 9).

Next to the large-scale overturning circulation, also local processes are present. One such process is boundary mixing, which occurs in the near–bottom region. Boundary mixing is a major contributor to the vertical transport of salt, heat, and matter across the whole basin, whether it be a basin the size of the Baltic Sea, a small lake or the World Ocean (Holtermann et al., 2014, and references therein). Despite its importance, the quantification of boundary mixing has been a challenging task. Recent advances on the subject, such as the modeling study by Holtermann et al. (2014), have been made possible by (i) the implementation of a vertically adaptive numerical grid that resolves the bottom boundary layer (Hofmeister et al., 2010), and (ii) by state–of–the–art turbulence models (Umlauf & Burchard, 2005). The modeling study by Holtermann et al. (2014) is motivated by their previous results from observation data of the Baltic Sea Tracer Release Experiment (Holtermann et al., 2012; Holtermann & Umlauf, 2012). In the early work by Garrett (1990), the role of bidirectional flow in boundary mixing was investigated. An idealized one–dimensional model was used by Umlauf and Burchard (2011) to investigate how shear, stratification and turbulence interact in the boundary layer on sloping topography. Their velocity profile showed an exchange flow with up–slope velocity near the bottom, and down–slope velocity above (Umlauf & Burchard, 2011, their Fig. 5). The consensus in 2016 on the global abyssal overturning circulation misses a key point

according to Ferrari et al. (2016). They argue that recent observations prior to their study had shown bottom-intensified mixing in abyssal waters, and that this is not considered in the theory. The enigma that arises when considering these measurements in the light of the theory, is that a reversed picture emerges. These measurements indicate that waters should sink due to the increased mixing, but the theory considers rising water masses. Therefore, they strongly argue for the inclusion of bottom–intensified mixing in the theory. Their proposal to accommodate for this missing point, is that the abyssal waters ascend to the surface along thin, turbulent bottom boundary layers. In this paper, we carry out a three-dimensional numerical model study and investigate the boundary mixing in an isohaline framework, comprising both features (i) and (ii) mentioned above.

The theory of the isohaline framework is based on the water mass transformation (WMT) framework. WMT was introduced by Walin (1977, 1982), originally, in the former work, for the description of estuaries. In a recent review by Groeskamp et al. (2019), a more general WMT is discussed. WMT is defined in Groeskamp et al. (2019) as the "mass transport of seawater through a surface with a constant property value". The benefit of WMT is that it provides an indirect means of studying the ocean circulation based on tracers. This way of indirectly analyzing the ocean circulation complements direct measurements. Air–sea fluxes and mixing are the main processes causing water mass transformation (Groeskamp et al., 2019). The study by Walin (1977) introduced a WMT framework using salinity as an essential scalar property for a WMT analysis of the Baltic Sea. Further studies used WMT in thermohaline coordinates to study the thermohaline ocean circulation (Döös et al., 2012; Zika et al., 2012; Groeskamp et al., 2014). The meridional circulation cells in the Southern Ocean were studied using WMT in the form of overturning stream functions in latitude–density space (Döös & Webb, 1994). In the later study by Döös et al. (2004), the overturning circulation of the Baltic Sea is viewed by using meridional stream functions as functions of the four vertical coordinates depth, salinity, temperature and density. While the TEF analysis framework studies the exchange flow at individual transects in space, the stream function as shown in Döös et al. (2004) makes it possible to illustrate the circulation by concatenating the TEF profiles from different transects.

All the methods presented up to this point are important diagnostic tools to study estuarine dynamics. In particular, maps of diahaline velocity and diffusive salt fluxes, as seen in Wang et al. (2017) and Li et al. (2022), allow for studying the link between mixing and diahaline exchange flow. Recently, Klingbeil and Henell (2023) derived a *local* Water Mass Transformation framework and provided exact definitions for local diasurface quantities. Moreover, they derived relations between these quantities, thereby generalizing the formulations by Li et al. (2022). In particular, they provided an equation that directly formulates how small-scale mixing, i.e. local dissipation of tracer variance, is associated with the local dia-surface exchange flow. In this paper we verify these local relations for the first time in an isohaline framework using a realistic model for the non-tidal, fjord-type Baltic Sea. The use of an isohaline framework to study the circulation in salinity space is particularly appropriate since the density–driven estuarine circulation is mainly controlled by the salinity gradient. We quantify local and integrated contributions to the diahaline volume transport, diahaline diffusive salt transport and diahaline mixing. Moreover, we separate the mixing into physical and numerical contributions and quantify the associated physical and numerical diahaline exchange flow. With our local diagnostics we investigate diahaline boundary mixing in detail and contribute to existing theories on boundary mixing.

This paper has the following structure. First, it introduces the applied methods in Section 2. Therein, the theory of the isohaline framework is described, focusing on the diahaline quantities presented in this work. This section further includes a description of the study area that the theory is applied to, and of the numerical model used to produce the results. The results are presented in seven subchapters on the *(i)* hydrographic

state, *(ii)* diahaline volume transport, *(iii)* diahaline diffusive salt transport, *(iv)* diahaline mixing, *(v)* relations between the diahaline quantities, *(vi)* physically and numerically induced diahaline exchange flow, and *(vii)* a more detailed view on boundary mixing. Concluding remarks are made concerning new insights into the isohaline framework, and further applications of this method are discussed in Section 4.

2 Methods

2.1 Budgets and relations in salinity space

Adapting the general equations (18) and (26) from Klingbeil and Henell (2023) to salinity yields

$$\frac{\partial D_\leq(S)}{\partial t} + \frac{\partial U_\leq(S)}{\partial x} + \frac{\partial V_\leq(S)}{\partial y} + u_{\mathrm{dia,z}}(S) = P - E, \tag{1}$$

$$\frac{\partial S_\leq(S)}{\partial t} + \frac{\partial F_{\mathrm{x},\leq}(S)}{\partial x} + \frac{\partial F_{\mathrm{y},\leq}(S)}{\partial y} + f_{\mathrm{dia,z}}(S) = 0. \tag{2}$$

These budgets describe how the thickness $D_\leq(S)$ and salt content $S_\leq(S)$ of all water with salinities smaller or equal to S in an individual water column evolve in terms of the divergence of horizontal transports with salinities $\leq S$, diahaline fluxes (per unit horizontal area) across the isohaline with salinity S, and surface freshwater fluxes due to precipitation (P) and evaporation (E). The diahaline salt flux in (2) consists of advective and diffusive contributions:

$$f_{\mathrm{dia,z}}(S) = S u_{\mathrm{dia,z}}(S) + j_{\mathrm{dia,z}}(S). \tag{3}$$

Exact mathematical expressions for $u_{\mathrm{dia,z}}(S)$ and $f_{\mathrm{dia,z}}(S)$ have been derived in Klingbeil and Henell (2023, their (20) and (30)), but are not required in this study, because they will be diagnosed from (1) and (2). Mathematically, the cumulative quantities in (1) and (2) are defined by vertical integration over the parts of the water column where the salinity is $\leq S$,

$$D_\leq(S) = \int_{S(z)\leq S} \mathrm{d}z \qquad\qquad U_\leq(S) = \int_{S(z)\leq S} u(z)\,\mathrm{d}z, \tag{4}$$

$$S_\leq(S) = \int_{S(z)\leq S} S(z)\,\mathrm{d}z \qquad\qquad F_{\mathrm{x},\leq}(S) = \int_{S(z)\leq S} f_{\mathrm{x}}(z)\,\mathrm{d}z, \tag{5}$$

with u and f_{x} being the zonal velocity and salt flux (accordingly for the transports in y-direction). Analogously, a cumulative salinity mixing can be defined as

$$M_\leq(S) = \int_{S(z)\leq S} \chi(z)\,\mathrm{d}z, \tag{6}$$

with the salinity variance dissipation rate

$$\chi = 2\left(K_{\mathrm{h}}\left(\frac{\partial S}{\partial x}\right)^2 + K_{\mathrm{h}}\left(\frac{\partial S}{\partial y}\right)^2 + K_{\mathrm{v}}\left(\frac{\partial S}{\partial z}\right)^2\right) \tag{7}$$

associated with salinity diffusion by horizontal and vertical diffusivities K_{h} and K_{v}, respectively. From (6) the mixing per (infinitesimal) salinity class is obtained as

$$m(S) = \frac{\partial M_\leq(S)}{\partial S}. \tag{8}$$

An intuitive view of the local diahaline fluxes and mixing is given in a sketch of an idealized estuary in Fig. 2c. The sign convention applied in this work is described in Fig.

2a,b. Klingbeil and Henell (2023) showed how, under the assumption of negligible horizontal diffusive salt fluxes and no sources and sinks, the following simple relations between the diahaline quantities can be derived (their (46), (40) and (47)):

$$u_{\text{dia,z}}(S) = -\frac{\partial j_{\text{dia,z}}(S)}{\partial S}, \tag{9a}$$

$$j_{\text{dia,z}}(S) = -\frac{1}{2}m(S), \tag{9b}$$

$$u_{\text{dia,z}}(S) = \frac{1}{2}\frac{\partial m(S)}{\partial S}. \tag{9c}$$

To which extent the relations (9a)–(9c) hold in realistic applications has to be investigated. Integrated diahaline quantities can be obtained by horizontal integration over all water columns,

$$Q_{\text{dia}}(S) = \int u_{\text{dia,z}}(x, y, S)\,\mathrm{d}x\,\mathrm{d}y, \tag{10a}$$

$$\mathcal{J}_{\text{dia}}(S) = \int j_{\text{dia,z}}(x, y, S)\,\mathrm{d}x\,\mathrm{d}y, \tag{10b}$$

$$\mathtt{m}(S) = \int m(x, y, S)\,\mathrm{d}x\,\mathrm{d}y, \tag{10c}$$

and the integral formulations of the relations (9a)–(9c) read

$$Q_{\text{dia}}(S) = -\frac{\partial \mathcal{J}_{\text{dia}}(S)}{\partial S}, \tag{11a}$$

$$\mathcal{J}_{\text{dia}}(S) = -\frac{1}{2}\mathtt{m}(S), \tag{11b}$$

$$Q_{\text{dia}}(S) = \frac{1}{2}\frac{\partial \mathtt{m}(S)}{\partial S}. \tag{11c}$$
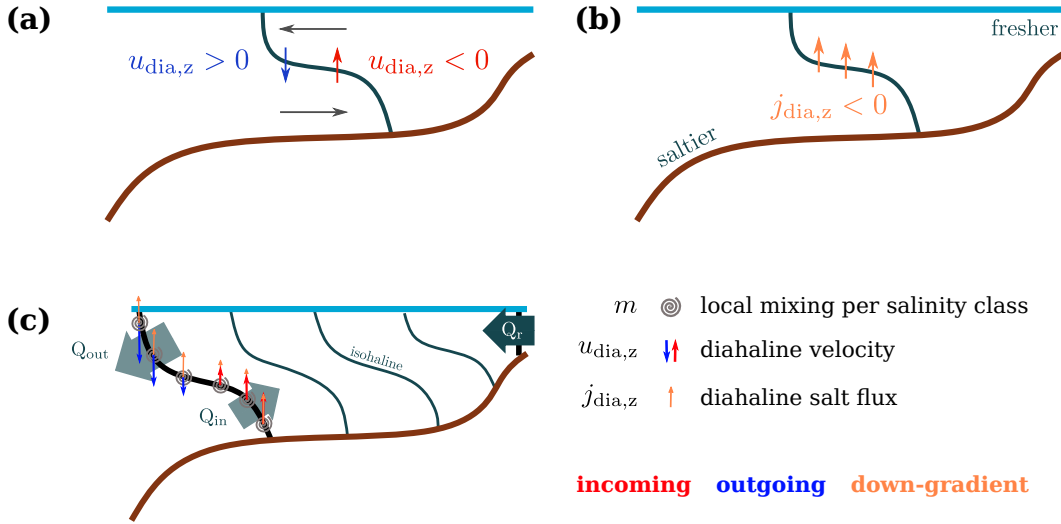

Figure 2. Sketch for an idealized estuary displaying the sign convention for (a) the effective vertical diahaline velocity $u_{\text{dia,z}}$ and (b) the effective vertical diahaline diffusive salt flux $j_{\text{dia,z}}$. Diahaline fluxes are counted positive into the direction of increasing salinity. Therefore, negative diahaline velocity is counted as incoming, and positive diahaline velocity as outgoing. (c) Sketch visualizing the location of the terms in relations (9a)–(9c).

2.2 Study area

In the present study, we demonstrate the analytical power of relations (9a)–(9c) for the estuary of the Baltic Sea, because a detailed understanding of diahaline processes is highly relevant for its ecosystem.
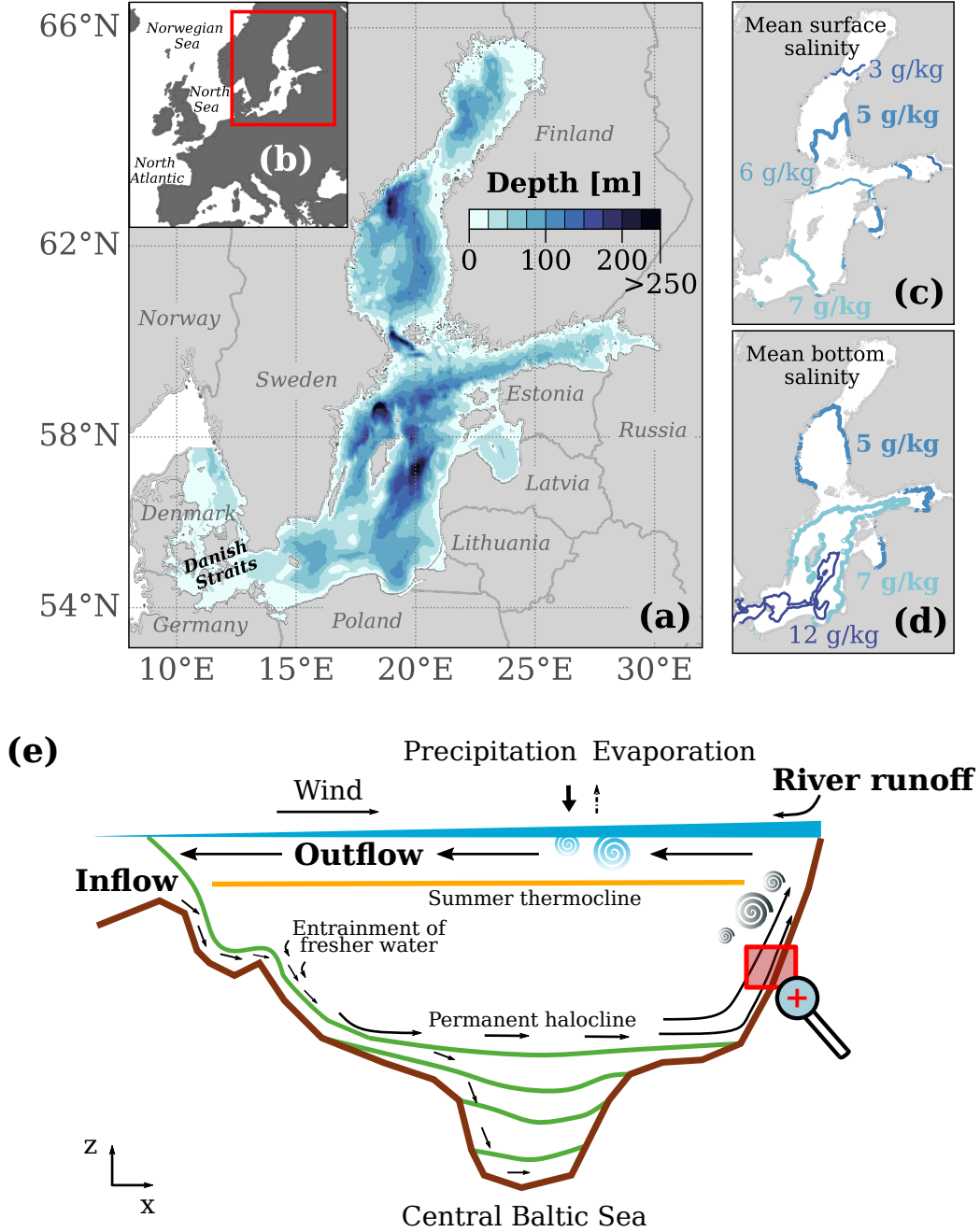

Figure 3. (a) Bathymetric map of the Baltic Sea. (b) Location of the Baltic Sea in Europe. (c) Mean surface salinity contour lines for 3, 5, 6 and 7 g/kg. (d) Mean bottom salinity contour lines for 5, 7 and 12 g/kg. (e) Schematic of the water balance and overturning circulation in the Baltic Sea in longitude–depth space based on Matthäus (2006, his Fig. 1.2). The magnifying glass refers to Sec. 3.7 and Fig. 14 where diahaline boundary mixing is studied.

The Baltic Sea is an almost non-tidal marginal sea located in northern Europe, and bounded by the European main continent and Scandinavia. The only connection to the North Sea (and the World Ocean) is established through the narrow and shallow Danish Straits (see Fig. 3a). The catchment area of the Baltic Sea includes many rivers with the largest river runoff originating from the Neva river near St. Petersburg in Russia (Bergström & Carlsson, 1994). This fresh river runoff, and precipitation, in the surface waters mix with the saline and dense Atlantic waters flowing in through the straits, and result in a net outflow of the mixed, brackish waters towards the North Sea. An exchange flow is formed. For this circulation – consisting of the inflow of salty, dense bottom waters, upwelling and mixing with fresh surface waters, and outflow of brackish waters in the upper water layers – Döös et al. (2004) coined the term "Baltic Haline Conveyor Belt".

A prominent feature of the Baltic Sea is the halocline at 40–80 m depth in the deeper basins (Liblik & Lips, 2019), from which ensues a permanent salinity stratification. This halocline serves as an efficient delimiter between surface and bottom water masses. A general idea of how the isohalines are located in the Baltic Sea is given by displaying the mean surface and bottom salinity of, respectively, isohalines 3, 5, 6 and 7 g/kg in the former, and 5, 7 and 12 g/kg in the latter case (Fig. 3c,d). In addition to the permanent halocline, a seasonal thermocline between depths of 10–30 m develops during the summer months (Reissmann et al., 2009), see Fig. 3e. The bathymetry of the Baltic Sea contains several basins such as the Arkona Basin, the Bornholm Basin and the Gotland Basin. Of these, the Gotland Basin is the deepest with a depth of 459 m in its western and 248 m in its eastern branch. The mean depth of the Baltic Sea, however, is only at about 52 m.

The inflowing saline water is dense, therefore heavy, and also oxygen-rich, and thus ventilates the deeper basins of the Baltic Sea. These inflows are the main source of deep-water salt and oxygen in the Baltic Sea and are therefore important for the Baltic Sea ecosystem and its maintenance. The only other source of oxygen is from diffusive flux at the sea surface, which can not enter the deeper basins efficiently due to the strong vertical stratification (Döös et al., 2004; Mohrholz et al., 2015). The inflows can be either more frequent medium–intensity salinity inflow events from the Kattegat, or less frequent major barotropic and baroclinic inflow events (MBIs). The occurrence of the inflow events is linked to the weather patterns over this region. The *barotropic* inflow events are forced by the differences in sea level between the Arkona Basin and the Kattegat due to wind and air pressure forcing (Franck et al., 1987; Wyrtki, 1954; Matthäus, 2006). This type of inflow is more frequent during the winter season, but may also occur during the other seasons. *Baroclinic* inflows, on the other hand, are driven by the density gradient between the Kattegat and the Baltic, and are common during long and calm summer periods (Knudsen, 1900; Hela, 1944; Feistel, Günther, et al., 2003; Feistel, Nausch, et al., 2003; Feistel et al., 2006; Mohrholz et al., 2006).

A detailed review of current knowledge gaps concerning the Baltic Sea, with special emphasis on its salinity dynamics, has been provided by Lehmann et al. (2022). Among other things, they emphasize the lack of knowledge about regional coastal processes and small-scale variability. They also point out that we do not yet understand all branches of the general circulation of the Baltic Sea. The methods applied in our work serve to better understand the Baltic Sea circulation and mixing hotspots, which in turn may be useful for understanding different branches of the circulation. In addition, it provides insight into possible future research opportunities, e.g. by applying the isohaline framework to improve knowledge of MBIs.

2.3 Numerical model

Realistic numerical simulations of the Baltic Sea have been carried out with the General Estuarine Transport Model (GETM; Burchard and Bolding (2002), Klingbeil

and Burchard (2013)). GETM is an open source three-dimensional coastal ocean model. General details about the numerics can be found in Klingbeil et al. (2018). A special feature of GETM are vertically adaptive model layers (Hofmeister et al., 2010). Their automatic zooming towards areas of strong stratification significantly reduces spurious numerical mixing and is fundamental for the proper simulation of the halocline in the Baltic Sea (Gräwe et al., 2015). GETM supports the separate quantification of physical mixing due to turbulence parameterizations and spurious numerical mixing due to discretization errors of the advection schemes according to Klingbeil et al. (2014). In each grid cell the variance decay caused by tracer diffusion (χ_{phy}) and tracer advection (χ_{num}) is diagnosed. The changes of salinity variance due to river discharge, precipitation and evaporation are also counted as "physical" contributions, such that χ_{num} solely contains the spurious effects of the numerical advection scheme. For the present study, GETM was extended to also diagnose the effective vertical diahaline velocity $u_{\mathrm{dia,z}}(S)$ from (1), the effective vertical diahaline diffusive salt flux $j_{\mathrm{dia,z}}(S)$ by means of (3) from (2), as well as the physical and numerical mixing per salinity class $m_{\mathrm{phy}}(S)$ and $m_{\mathrm{num}}(S)$ from (8), respectively. For every water column the required cumulative quantities (4)–(6) are obtained after binning the layer heights, transports, salt contents and variance decay from the model grid cells into equidistant salinity bins of size 0.2 g/kg. All transports are binned based on the corresponding interface salinity given by an upwind approximation.

The model setup with a spatial resolution of approximately 1 nautical mile is described and validated in Burchard et al. (2018) and Gräwe et al. (2019). The simulated time period covers the years of 2014 and 2015, with a measured MBI event occurring at the end of 2014 (Mohrholz et al., 2015). A temporal average was taken over these two years.
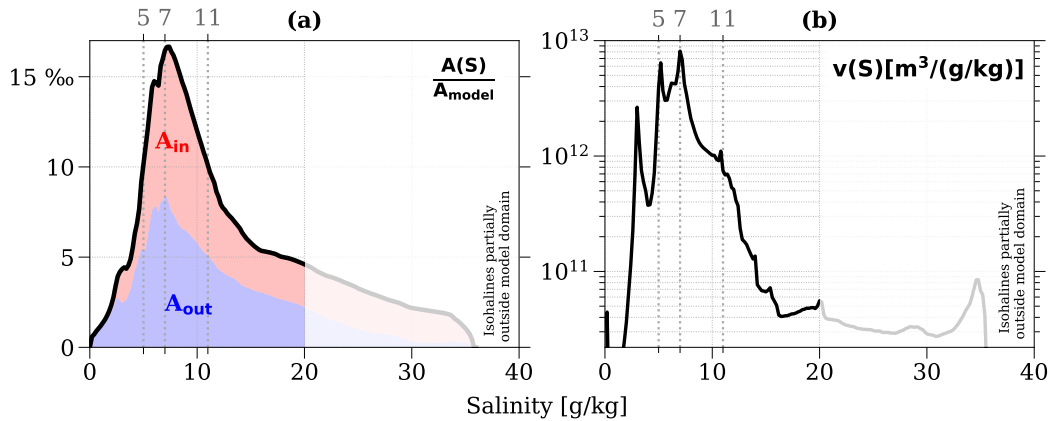
3 Results

3.1 Hydrographic state

Figure 4. Isohaline area $A(S)$ and volume per salinity class $v(S)$ are shown in (a) and (b), respectively. The isohaline area is the respective surface covered by every present isohaline. The isohaline volume is the total volume encompassed by the respective salt class. A_{in} is the isohaline surface of the incoming, and A_{out} of the outgoing flow, calculated by means of (14). The paler patch shows the isohalines already extending outside the model domain, and thus do not account for all near surface areas across which outflow occurs. This is the intermediate case 2 in Fig. 1.

The isohaline surface $A(S)$ and the isohaline volume per salinity class $v(S)$ serve as means of describing the hydrographic state of the Baltic Sea (Walin, 1977). Due to the small slope of the isohalines, the isohaline surface can be approximated by the horizontal footprint area of all water columns, where the particular isohaline is present. The isohaline volume per salinity class is defined as follows:

$$v(S) = \frac{\partial V(S)}{\partial S}, \tag{12}$$

where $V(S)$ is the volume of all water with salinity smaller than or equal to a specific salinity S. The mean isohaline surface, scaled with the area of the entire Baltic Sea, is shown in Fig. 4a, and the isohaline volume per salinity class in Fig. 4b. Both quantities have a maximum at a salinity of 7 g/kg, with a sharp increase prior and a slower decrease after the peak. This result can be expected since the 7 g/kg isohaline accounts for the surface water in large parts of the central Baltic Sea. For salinities larger than 20 g/kg the isohalines (partially) and the isohaline volumes extend outside the model domain. This corresponds to the intermediate case in Fig. 1.

3.2 Diahaline volume transport

Maps of the effective vertical diahaline velocity are shown in Fig. 5. Note, that in all plots the effective vertical diahaline velocity is labeled diahaline velocity for brevity. All maps show the general picture of outgoing volume transport towards higher salinity classes in the south/southwestern, and incoming volume transport towards lower salinity classes in the northern/northeastern extent of the corresponding isohalines. This diahaline overturning circulation complements the classical picture of estuarine circulation with salty bottom inflow and brackish surface outflow sketched in Fig. 2c.

To investigate this exchange flow further, we study the integrated incoming and outgoing diahaline transports:

$$\begin{aligned} Q_{\text{dia}}^{\text{in}}(S) &= -\int_{u_{\text{dia,z}}(x,y,S)<0} u_{\text{dia,z}}(x,y,S) \, dx \, dy \\ Q_{\text{dia}}^{\text{out}}(S) &= +\int_{u_{\text{dia,z}}(x,y,S)>0} u_{\text{dia,z}}(x,y,S) \, dx \, dy. \end{aligned} \tag{13}$$

The integrals in (13) only integrate over areas with negative $u_{\text{dia,z}}$ for $Q_{\text{dia}}^{\text{in}}$, and areas with positive $u_{\text{dia,z}}$ for $Q_{\text{dia}}^{\text{out}}$, respectively. Similarly, we compute the areas of the isohalines where inflow and outflow are occurring:

$$\begin{aligned} A_{\text{in}}(S) &= \int_{u_{\text{dia,z}}(x,y,S)<0} dx \, dy \\ A_{\text{out}}(S) &= \int_{u_{\text{dia,z}}(x,y,S)>0} dx \, dy, \end{aligned} \tag{14}$$

The integrated diahaline transports are shown in Fig. 6. The incoming as well as the outgoing diahaline transport show a symmetric spread with a net dominance of outgoing transports caused by the freshwater supply due to rivers and net precipitation. The strongest diahaline exchange flow with maximum in- and outflowing transports occurs across the isohaline with the largest area (salinity 7 g/kg, see Fig. 4a).

This is different to many tidal estuaries where the strength of the exchange flow increases towards the highest salt classes, situated at the outlet of the estuary (see e.g. Fig. 4c,d in Li et al. (2022); Reese et al. (2023)). The incoming diahaline transport and the isohaline area where inflow occurs (see Fig. 4a) disappear towards lower salinities, where the outflow due to freshwater river discharge dominates. The diahaline transport at higher salinities mainly depicts the near bottom inflow, and misses the near surface
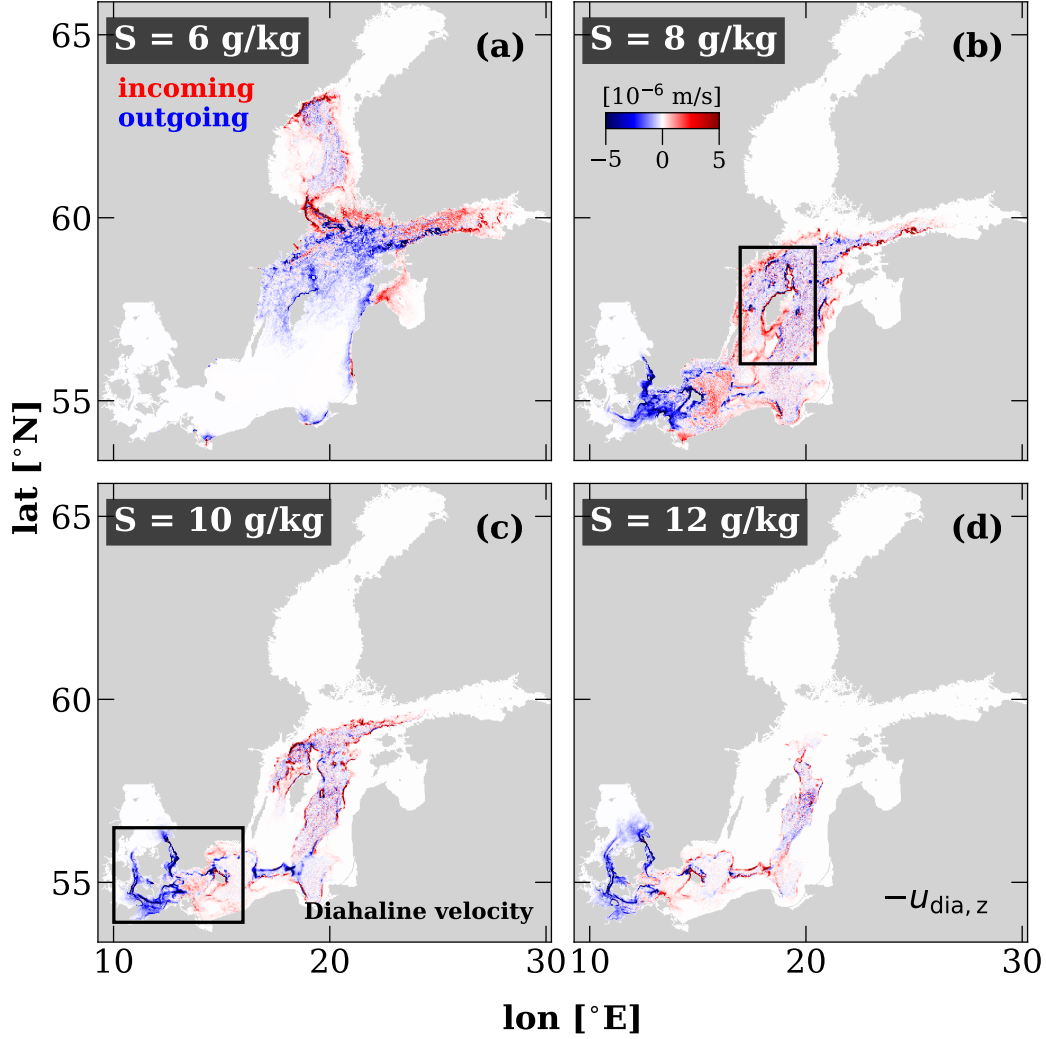
Figure 5. Maps of the effective vertical diahaline velocity, averaged over two years, across the isohalines of (a) 6, (b) 8, (c) 10, and (d) 12 g/kg. For the adopted sign convention, the reader is referred to Fig. 2a. The black boxes in panels (b) and (c) show the location of the zoomed–in regions of Fig. 12a, b, respectively.

outflow across the portions of the isohaline area that are already outside the model domain (see paler patch in Fig. 6 and reduced A_{out} in Fig. 4a). Except for the missing outflow for high salinities and the diahaline exchange flow inside the non-tidal basins across isohalines of intermediate salinities, the residual integrated diahaline transport agrees very well with the net freshwater supply. This net outflow is associated with a generally dominating isohaline area across which outflow occurs (Fig. 4a). Deviations between the mean freshwater supply and the residual integrated diahaline transport are expected, because time averaged results from our only 2 year long simulation period (including a Major Baltic inflow event) cannot represent a long-term balanced state of the Baltic.

In this study we have chosen to focus our analysis on three salt classes. The salt classes of 5, 7 and 11 g/kg were picked as they cover the most relevant domains for the exchange flow. Moreover, they follow as a natural choice from the results of the isohaline area, isohaline volume per salinity class and diahaline transport (respectively Figs.
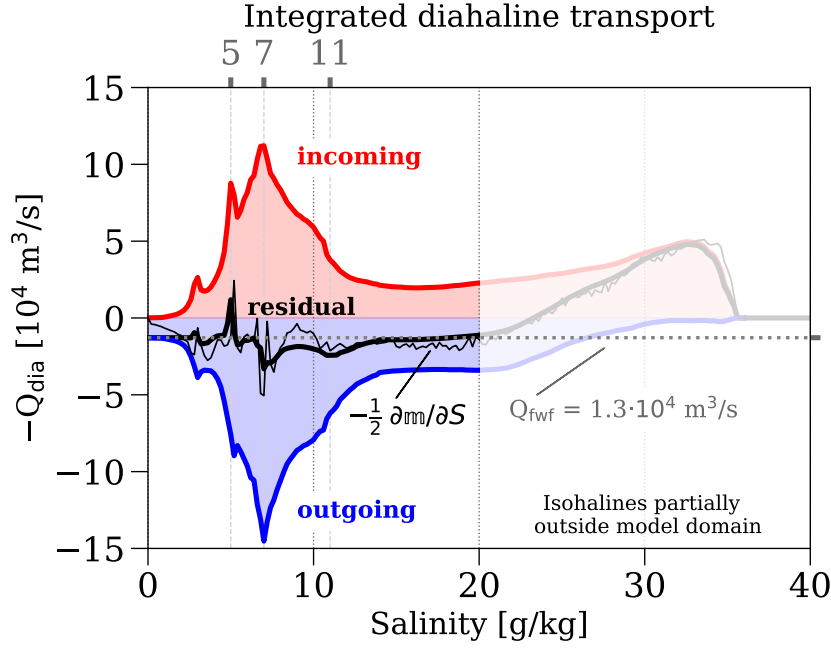
Figure 6. Integrated diahaline volumes transports. Incoming and outgoing contributions $Q_{\mathrm{dia}}^{\mathrm{in/out}}$ from (13) are shown in red and blue, respectively. The residual transport (thick black line) is identical to Q_{dia} from (10a). The dotted horizontal grey line is the net freshwater supply Q_{fwf} due to river discharge, evaporation and precipitation. The thin black line displays the derivative of the integrated mixing per salinity class m with respect to salinity, with m from (10c). It correlates with Q_{dia} (thick black line) with R=0.95 and indicates the approximate validity of relation (11c). The paler patch shows the isohalines already extending outside the model domain, and thus do not account for all near surface outflow anymore. This is the intermediate case 2 in Fig. 1.

4 and 6). The salt class of 7 g/kg, in particular, proved to be the location of the maximum in these analyses.

3.3 Diahaline diffusive salt transport

Maps of the effective vertical diahaline diffusive salt flux, averaged over two years, are shown in Fig. 7 a–c for salt classes 5, 7 and 11 g/kg. Note, that in all plots the effective vertical diahaline diffusive salt flux is labeled diahaline diffusive salt flux for brevity. Mostly a down–gradient diffusive salt flux ($j_{\mathrm{dia,z}} < 0$) is diagnosed across the three isohalines. In some areas very weak up-gradient diffusive salt fluxes are present, caused by the applied anti-diffusive advection schemes in the numerical model. The strongest effective diahaline diffusive salt fluxes occur across the isohaline of 11 g/kg in the surface waters of the shallow Western Baltic Sea and in the Danish Straits towards the North Sea where wind and tidal mixing dominate. In addition, the diffusive salt flux is enhanced along certain coastlines and bathymetric features, where the isohalines are in contact with the bottom topography.
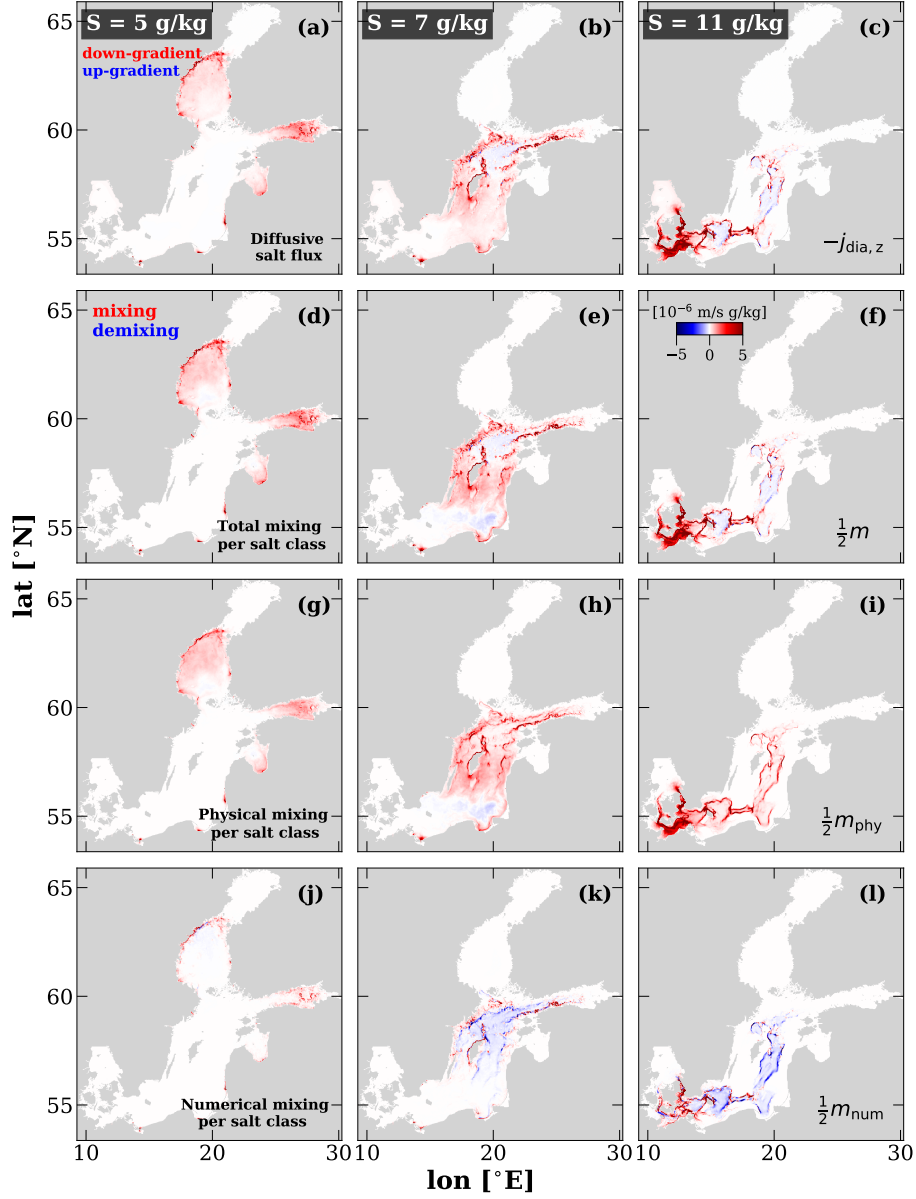
Figure 7. Maps of diahaline quantities averaged over two years. Column 1: salt class 5 g/kg; Column 2: 7 g/kg; Column 3: 11 g/kg. Row 1 (a–c): effective vertical diffusive salt flux; Row 2 (d–f): mixing per salinity class; Row 3 (g–i): physical mixing per salinity class; Row 4 (j–l): numerical mixing per salinity class. The almost identical patterns in panels a–c and d–f indicate the validity of relation (9b).

3.4 Diahaline mixing

Maps for the time-averaged local mixing per salinity class $m = m_{\mathrm{phy}} + m_{\mathrm{num}}$ across the respective isohalines are shown in Fig. 7 d–f. Mixing dominates over demixing for all three salt classes and leads to smoothed salinity gradients. Weak demixing tends to steepen the salinity gradients and occurs due to freshwater evaporation out of saline surface waters (counted as part of the physical mixing, see e.g. Fig. 7h) and due to the numerical advection schemes (see negative numerical mixing in Fig. 7k,l). The separation of the (total) mixing into physical and numerical contributions indicates that the simulation results are dominated by the physical mixing from the well-calibrated turbulence parameterization. The maps of physical and numerical mixing per salinity class (Fig. 7g–i,j–l) resemble similar patterns since both contributions depend on the salinity gradient. The mixing contributions are highest in the shallow areas of the Western Baltic Sea and in the tidally influenced Danish straits towards the North Sea (7i,l). All salinity classes show hotspots of physical and numerical mixing at the rims of the Baltic basins where the isohalines touch the bottom topography.
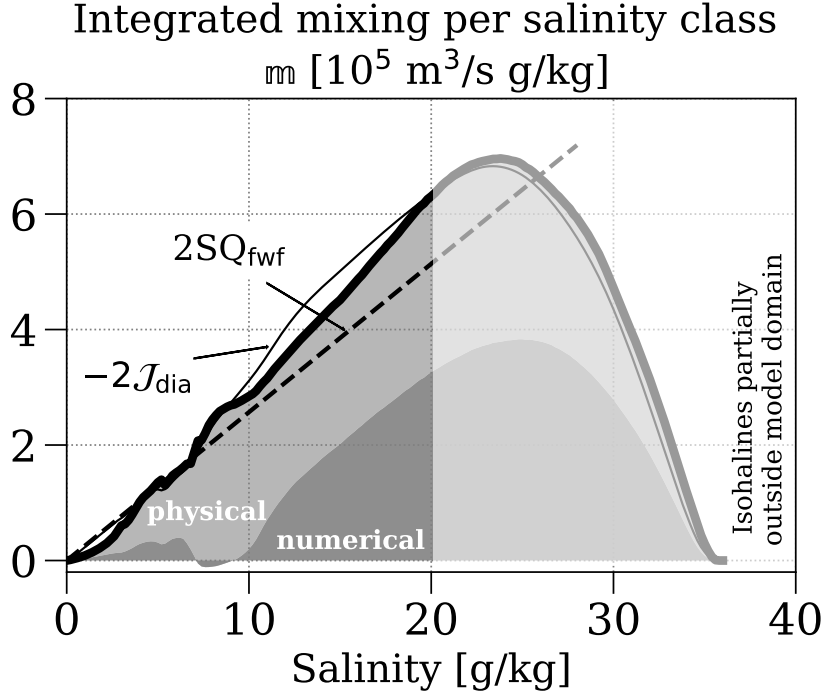

Figure 8. The integrated mixing per salinity class $\mathrm{m}(S)$ from (10c) is shown by the solid black line. The physical and numerical contributions are displayed in light and dark grey , respectively. The thin black line shows the integrated diahaline diffusive salt transport from (10b). It correlates with m with R=0.99 and indicates the validity of relation (11b). The dashed black line depicts the integrated mixing per salinitiy class following the universal law of estuarine mixing $\mathrm{m}(S) = 2SQ_{\mathrm{fwf}}$. The paler patch shows the isohalines already extending outside the model domain, where most of the mixing predicted by the universal law would happen. This refers back to intermediate case 2 in Fig. 1.

The integrated mixing per salinity class is presented in Fig. 8. This is the first time the integrated mixing per salinity class is shown for the Baltic Sea. A good agreement with the universal law of estuarine mixing $\mathrm{m}(S) = 2SQ_{\mathrm{fwf}}$ is shown for smaller salin-

ites up to 8 g/kg. For higher salinities, a deviation from the universal law is visible. This is because our temporal average of two years is not sufficiently long to remove the effects of varying volume and salt content on shorter time scales, which are not considered by the universal law. The turnover time of the Baltic Sea is around 25–30 years (Döös et al., 2004, and references therein), so a longer averaging period is expected to yield a better agreement with the universal law of estuarine mixing. Moreover, the deviation for salinities larger than 20 g/kg can be explained by the isohalines extending outside the model domain (intermediate case 2 in Fig. 1). For most salinity classes inside the Baltic Sea, the integrated mixing is dominated by physical mixing due to turbulence parameterization.

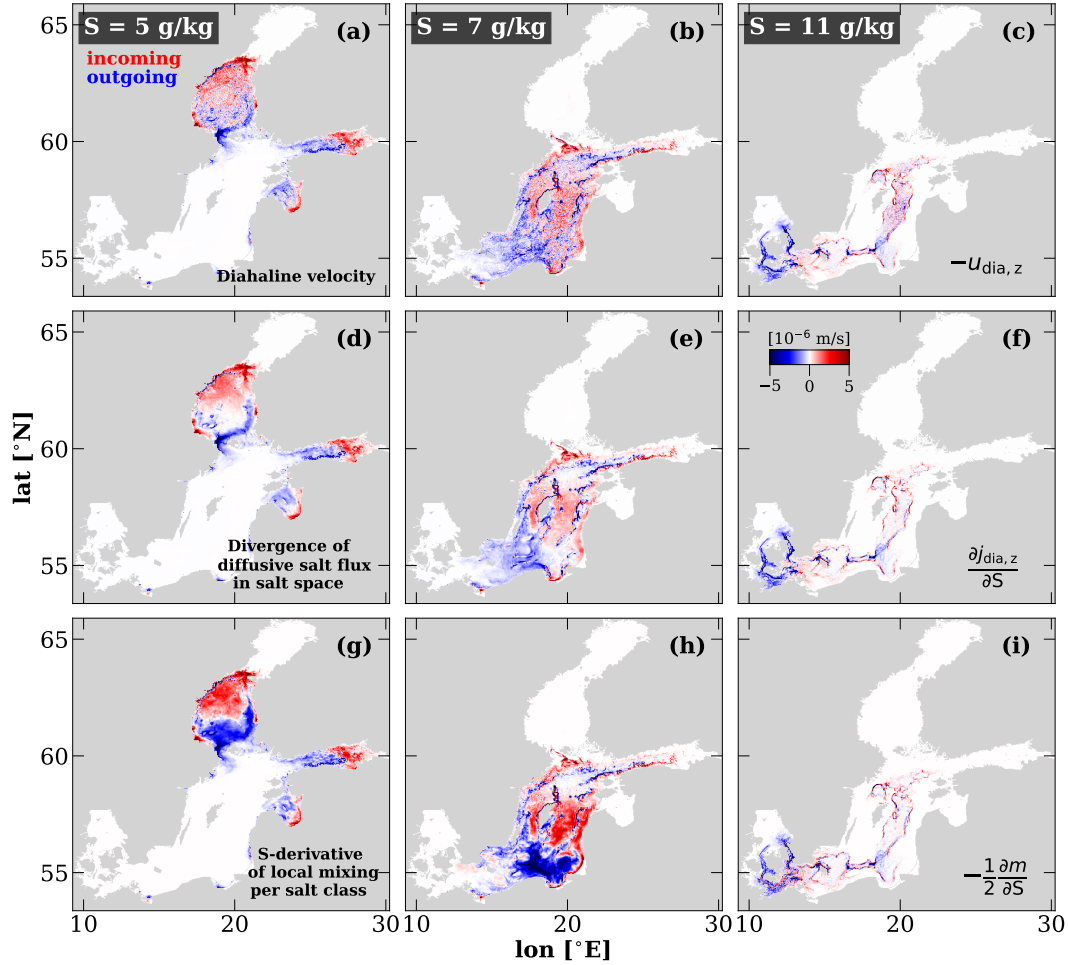### 3.5 Relations between diahaline quantitites

Figure 9. Maps of diahaline quantities averaged over two years. Column 1: 5 g/kg; Column 2: 7 g/kg; Column 3: 11 g/kg. Row 1 (a–c): effective vertical diahaline velocity; Row 2 (d–f): divergence of effective vertical diffusive salt flux in salt space; Row 3 (g–i): derivative of mixing per salinity class with respect to salinity. The similar patterns of the shown quantities for each isohaline indicate the approximate validity of the relations (9a)–(9c).

Here we analyze the validity of the relations (9a)–(9c). We do this by comparing the left and right hand side of each relation with each other.

Fig. 9 directly compares the diagnosed effective vertical diahaline velocity $u_{\mathrm{dia,z}}$ with the divergence of the diagnosed effective vertical diffusive salt flux in salinity space $\partial j_{\mathrm{dia,z}}/\partial S$, and with the derivative of the diagnosed mixing per salinity class with respect to salinity $\partial m/\partial S$ for different isohalines. For each isohaline the different quantities show very similar results, with the directly diagnosed effective vertical diahaline velocity appearing more noisy and $\partial m/\partial S/2$ being more pronounced.

The direct comparison of the diagnosed effective vertical diahaline diffusive salt flux $j_{\mathrm{dia,z}}$ with the mixing per salinity class m is presented in Fig. 7. The dominating patterns of strong fluxes and mixing are very similar, except for small areas of demixing caused by freshwater evaporation out of saline surface waters without corresponding upgradient diffusive fluxes.

Overall, Figs. 7 and 9 indicate that the analytical relations (9a)–(9c) hold well in a realistic model for the estuary of the Baltic Sea. The smoother fields for the effective vertical diahaline diffusive salt flux and the mixing per salinity class could be explained by the fact that their reconstruction is based on the calculation of gradients with respect to S instead of a direct calculation. Another reason could be horizontal diffusive salt fluxes present in reality and our numerical model. However, horizontal diffusive salt fluxes have been neglected during the derivation of the idealised analytical relations (9a) and (9c). Therefore, the directly diagnosed effective vertical diahaline velocity is less smooth and deviates from the analytical relations.

The maps of the diahaline quantities (Figs. 7 and 9) give a useful general view and portray the relations to hold well. A more quantitative evaluation is given by the scatter plots in Fig. 10. The correlations between the diahaline quantities are satisfying, because the deviations are caused by just a minority of data points. This is also confirmed by the excellent correlations between the integrated quantities. The relation (11a) between the integrated diahaline transport and the integrated diahaline diffusive salt flux fits perfectly with a correlation coefficient of R=1.0. The integrated diahaline diffusive salt flux and the integrated mixing per salinity class are compared in Fig. 8 and the correlation coefficient of relation (11b) is R=0.99. The relation (11c) between the integrated diahaline transport and the integrated mixing per salinity class is shown in Fig. 6. There, the derivative of the integrated mixing per salinity with respect to salinity is noisy, but it still correlates with R=0.95. With this, also the integral relations have been verified in a realisitic model for the estuary of the Baltic Sea.

3.6 Physically and numerically induced diahaline exchange flow

After having confirmed the validity of the relation (9c) between the effective vertical diahaline velocity and the mixing per salinity class, this relation can be used to calculate separate estimates for the physically and numerically induced portions of the diahaline exchange flow in terms of the physical and numerical mixing contributions (see Sec. 3.4 and Fig. 7g–l).

Fig. 11 compares the physically and numerically induced effective vertical diahaline velocities. In most areas the diahaline exchange flow across the presented isohalines is clearly dominated by physics, but it becomes clear that the role played by numerics is far from negligible. Both contributions show enhancement along the topographic boundaries.

By means of (13), also the physically and numerically induced integrated incoming and outgoing diahaline transports can be obtained (Fig. 11g, h). Interestingly, the resulting residual transports show opposite directions for the physical and numerical contributions across some isohalines, e.g. across 7 g/kg and 11 g/kg. Indeed, the integrated transports confirm that the physically induced contribution usually dominates the exchange flow across isohalines with salinities below 10 g/kg. However, for most isohalines
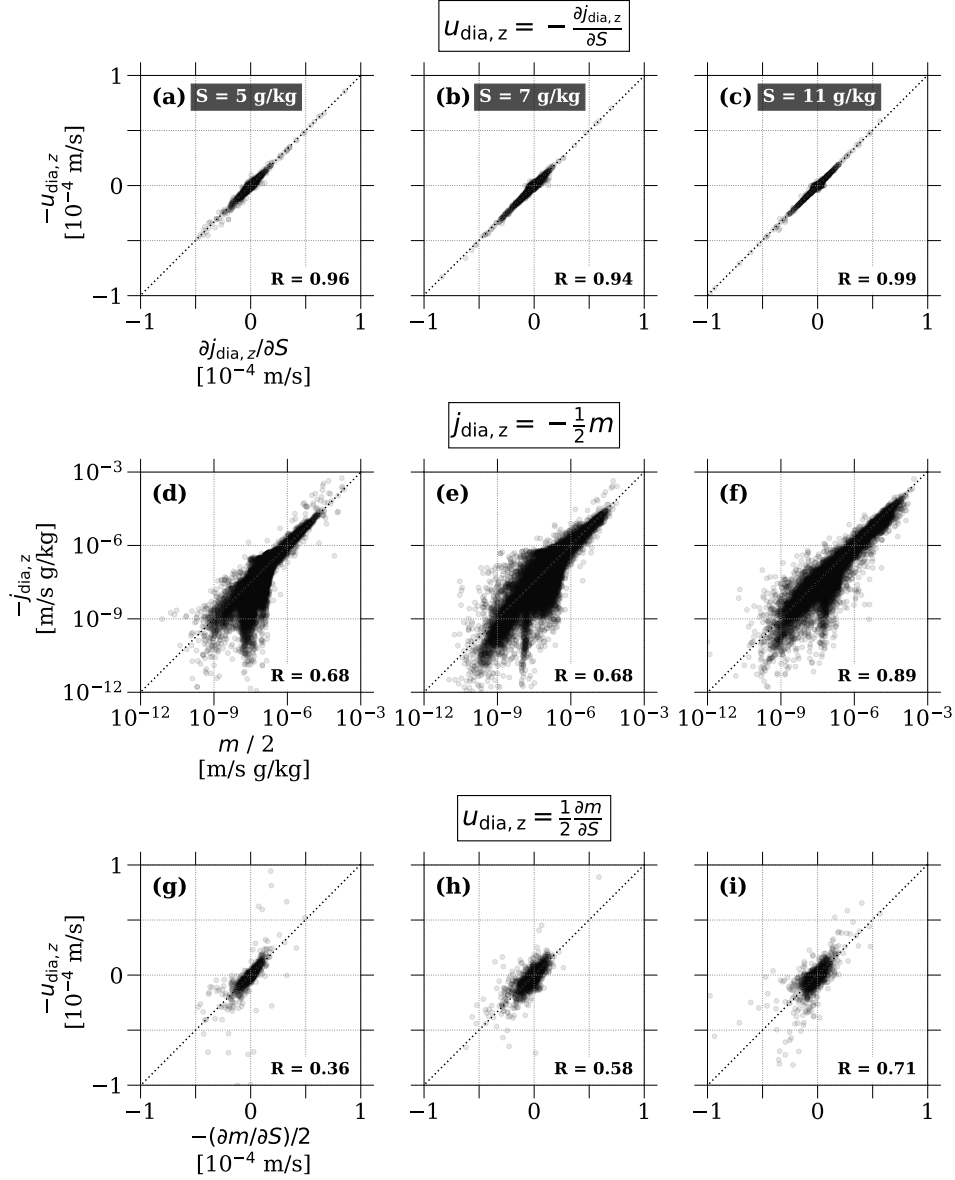
$$u_{\mathrm{dia},z} = -\frac{\partial j_{\mathrm{dia},z}}{\partial S}$$

$$j_{\mathrm{dia},z} = -\frac{1}{2}m$$

$$u_{\mathrm{dia},z} = \frac{1}{2}\frac{\partial m}{\partial S}$$

Figure 10. Scatter plots for the relations between the effective vertical diahaline velocity $u_{\mathrm{dia},z}$, the effective vertical diahaline diffusive salt flux $j_{\mathrm{dia},z}$ and the mixing per salinity class m. Left column: salinity class 5 g/kg; Middle column: salinity class 7 g/kg; Right column: salinity class 11 g/kg. First row: relation (9a); Second row: relation (9b); Third row: relation (9c). For every scatter plot the corresponding correlation coefficient R is included.

the numerically induced transports contributes with up to 50% and more to the diahaline exchange flow (Fig. 11i).

3.7 A more detailed view on boundary mixing

Several of the Baltic Sea maps presented in this work, e.g. Fig. 9b, highlight hot spots for diahaline boundary mixing. Where the mixing is stronger, also the mixing gradient is increased. By means of relation (9c) also the diahaline velocity is stronger at mix-
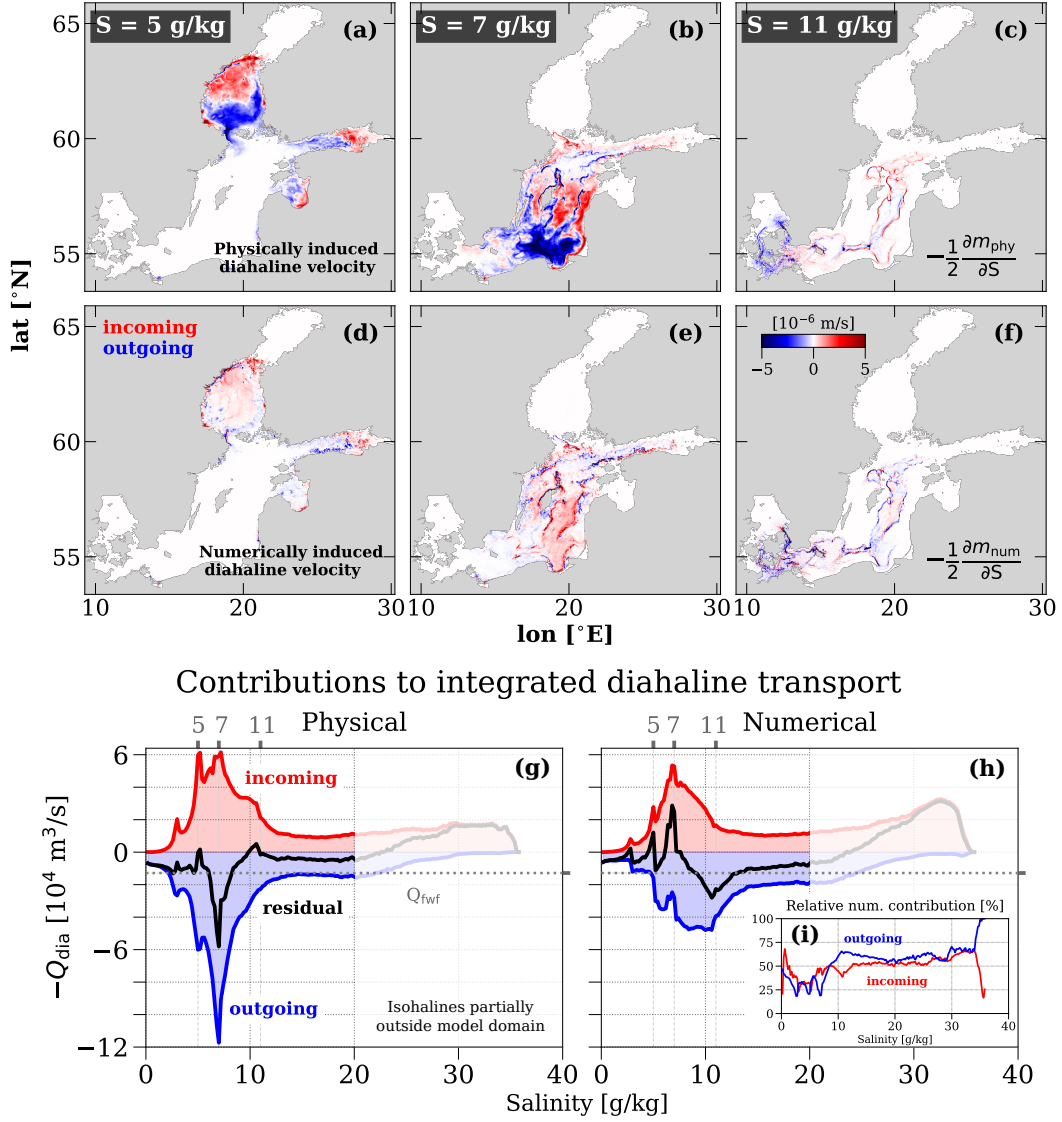
Figure 11. Maps of the physically (a–c) and numerically (d–f) induced effective vertical diahaline velocity, diagnosed by means of (9c) in terms of the two-year averaged physical and numerical mixing per salinity class, m_{phy} and m_{num}, respectively. Left column: salinity class 5 g/kg; Middle column: salinity class 7 g/kg; Right column: salinity class 11 g/kg. Physical (g) and numerical (h) contributions to the integrated diahaline transport, individually separated into incoming and outgoing portions, calculated from (9c). The relative contribution of the integrated numerical diahaline transport to the sum of the integrated physical and numerical diahaline transport is shown in (i).

ing hot spots. Therefore, we can study the diahaline velocity when investigating the boundary mixing. Two mixing hot spots are zoomed in on in Fig. 12a,b: the Gotland island in the former, and the Western Baltic Sea in the latter. Incoming velocities closest to land on an inner ring are shown along the north–western coastline of Gotland (Fig. 12a). The inner ring with incoming $u_{\mathrm{dia,z}}$ is followed by an outer ring with outgoing $u_{\mathrm{dia,z}}$. The same structure is more clearly observable close to the Swedish coast north of Gotland and around the small island of Gotska Sandön to the north–east of Gotland. Further-
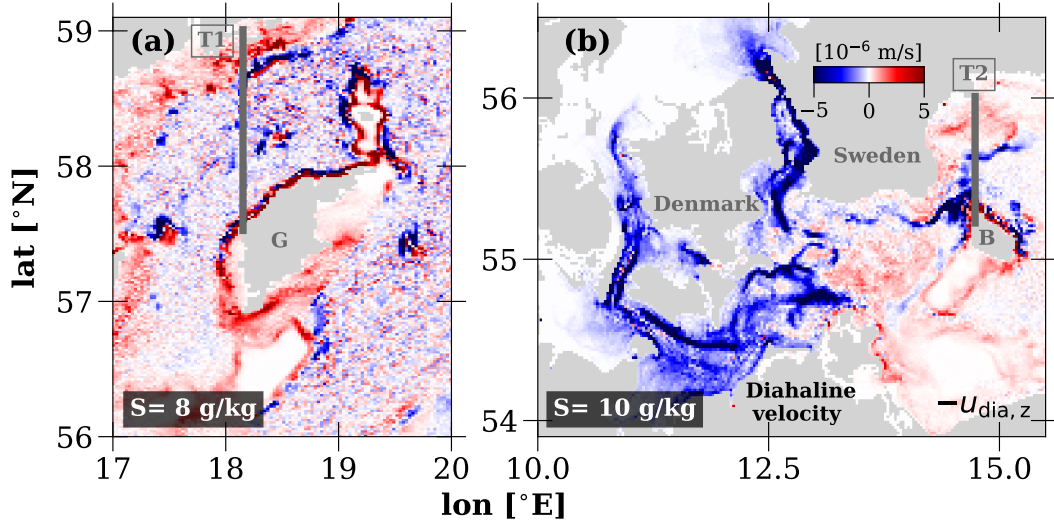
Figure 12. Zoom on the effective vertical diahaline velocity across the isohalines of 8 and 10 g/kg for (a) vicinity of Gotland island (G), and (b) Western Baltic Sea, respectively. For the location of the zoomed–in regions, see the rectangles in Fig. 9b,c. G: Gotland island, B: Bornholm island. A temporal average is taken over two years. Details along the transects T1 and T2 are shown in Fig. 13.

more, the seesaw pattern of an inner incoming velocity and outer outgoing velocity ring is present around the northern half of Bornholm island (Fig. 12b).

We investigate the pattern along two transects of local mixing per salinity class, derivative of mixing per salinity class and diahaline velocity (Fig. 13). The velocity transect is shown in latitude–depth and latitude–salinity space, the mixing and mixing gradient transect only in latitude–depth space. Mixing is showcased for the sake of a direct display of boundary mixing, without passing by relation (9c). A comparison of the mixing transects (Fig. 13a,b) with the velocity transects (Fig. 13e,f) confirms their appearance at the same locations. The similarity of the derivative of mixing per salinity class (Fig. 13c,d) and the effective vertical diahaline velocity (Fig. 13e,f) again confirm the validity of relation (9c) also in latitude–depth space along these transects. Transect 1 spans from the Gotland island with steeper bathymetry to the Swedish coast with flatter bathymetry (Fig. 13a,c,e,g). Transect 2 stretches from the Bornholm island to the southern Swedish coast (Fig. 13b,d,f,h). The location of the transects is displayed in Fig. 12. The isohalines included in z coordinates, and the isobaths included in S coordinates, connect the two spaces with each other, simplifying the interpretation and understanding of how they are connected. Regardless of the chosen space, the same structure is seen: a lower layer of incoming and an upper layer of outgoing velocities along the coasts. Consistent with the steep bathymetry of the Gotlandic coast, the observed structure is more spatially constrained. Off the flatter Swedish mainland coast, the two–layer structure is more spread out both horizontally as well as vertically. The isobaths in Fig. 13g reflect the different bathymetry in this region: they are denser off the Gotlandic coast with its steeper, and sparser off the Swedish mainland with its flatter topography. From transect 2, it is particularly visible how the S coordinates can be of use in visualizing and understanding the occurring processes: the incoming $u_{dia,z}$ in S coordinates between latitudes of 55.3 to 55.4 °N (Fig. 13h) covers a larger area than the same structure in z coordinates (Fig. 13f), and is thus easier to evaluate. Vertical integration of relation (9c) from minimum to maximum salinity, and noting that $m(S_{min}) = m(S_{max}) = 0$, shows
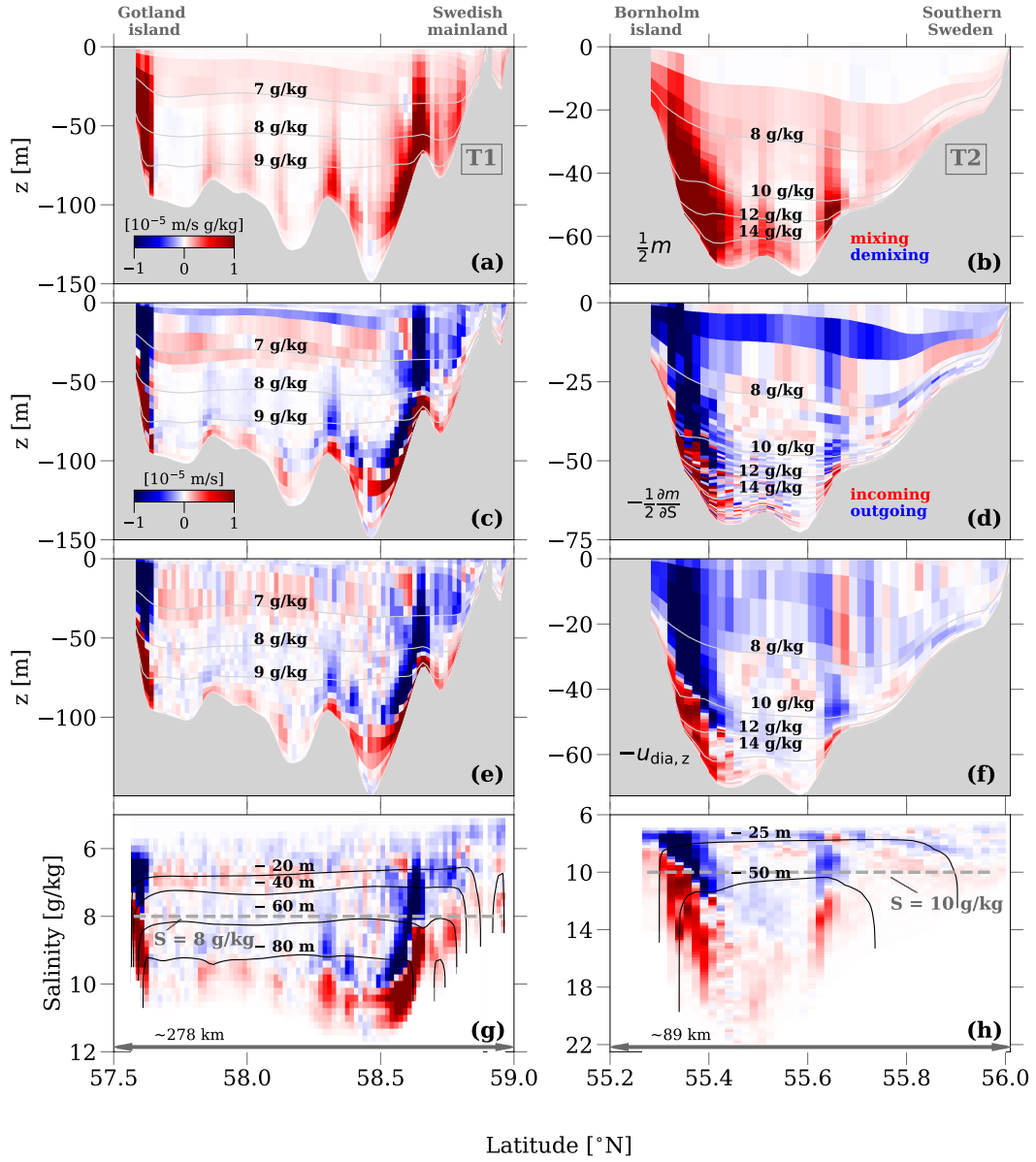
Figure 13. (a, b) Local mixing per salinity class, (c, d) derivative of the mixing per salinity class with respect to salinity, effective vertical diahaline velocity in (e, f) geopotential and (g, h) salinity space along the transects T1 and T2 shown in Fig. 12. A temporal average is taken over two years. Isohaline contour lines are included in (a)–(f), and isobathic contour lines in (g, h). Quantities in geopotential coordinates are obtained by consecutive arrangement of salt classes with their thicknesses, starting with lowest salinity at the ocean surface. The dashed grey lines in (g) and (h) correspond to the isohalines of 8 and 10 g/kg showcased in Fig. 12.

that the vertical S–integral of $u_{\mathrm{dia,z}}(S)$ must vanish. This can also be estimated from Figs. 13g,h. However, in fully physical space (Fig. 13e,f) this is generally not the case.
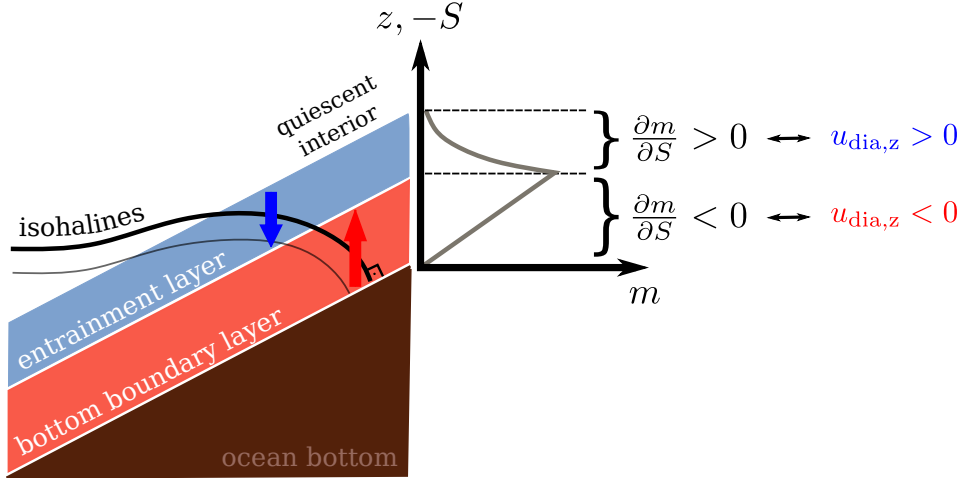
Figure 14. Sketch of the boundary mixing, adapted from Garrett (1990, his Fig. 1b) and Ferrari et al. (2016, their Fig. 2). The local link between mixing and exchange flow is visualized: they are connected through the relation (9c), which reads $u_{\text{dia,z}} = 1/2\ \partial m/\partial S$. For information on the sign convention used for the effective vertical diahaline velocity, see Fig. 2a.

4 Summary and conclusions

In this paper we have investigated the relation between the local diahaline quantities of mixing per salinity class, salt flux and velocity in a numerical model of a fjord–type, non–tidal estuarine system – the Baltic Sea. These quantities are connected with each other through newly derived, idealized relations in the earlier work by Klingbeil and Henell (2023). The bird's eye view in maps of local mixing per salinity class emphasizes the location of potential mixing hot spots. In these actively mixed regions the diffusive diahaline salt flux is also enhanced. The diahaline diffusive salt flux has the possibility to move water across the isohaline, and change the salinity of the transported water mass. Because the change in salinity is concurrent with mixing, the diahaline diffusive salt flux therefore gives information on where the mixing is occurring. The local diahaline velocity is a consequence of the diahaline diffusive salt flux, and the velocity itself determines the ensuing exchange flow. Thus goes the connection from local mixing per salinity class over diahaline diffusive salt flux to diahaline velocity: this is portrayed mathematically in relations (9a)–(9c). A good agreement was shown between the local diahaline quantities, implying that the relations hold well.

Transects of local mixing per salinity class and diahaline velocity in latitude–depth and latitude–salinity space are studied for a closer look at diahaline boundary mixing. Also close–up views of mixing hot spots were shown. From the transects and close–up views an identical pattern was inferred in latitude–depth/salinity space in the former and latitudinal direction in the latter case. Its characteristics consists of a seesaw structure for (i) incoming diahaline velocity and (ii) outgoing diahaline velocity: for the close–up maps in longitudinal direction an inner ring of (i), followed by an outer ring of (ii) is observed; for the transect in longitude–depth space (i) appears in the deeper and (ii) in the shallower layer; and for the transect in longitude–salinity space (i) occurs in the saltier and (ii) in the fresher layer. An idealized sketch of the Baltic overturning circulation in longitude–depth space, including main processes, is shown in Fig. 3e. A close–up view of the boundary processes is presented in Fig. 14, which is adapted from earlier sketches in the works of Garrett (1990, his Fig. 1b) and Ferrari et al. (2016, their Fig. 2). The isohalines are impinging at a right angle on the bottom in the bottom boundary layer.

This is a necessary condition to guarantee that no diffusive salt flux crosses the sloping boundary. In the bottom boundary layer an incoming, upward diahaline velocity is observed. Coherently, a negative mixing gradient is present. That is, the local mixing per salinity class increases with further distance from the bottom ($\partial m/\partial z > 0$), but salinity decreases, since it is highest directly at the bottom (if stably monotonic). Therefore, $\partial m/\partial S < 0$. The mixing gradient reaches a maximum, whereupon it decreases exponentially. The salinity continues to decrease since the water becomes fresher. From this results a positive mixing gradient, i.e. an outgoing, downward diahaline velocity. A result consistent with these findings has been obtained by Umlauf and Burchard (2011), who applied an idealized one–dimensional model for the oscillating bottom boundary layer over sloping topography. In their Fig. 5, they show profiles of up–slope velocity u and turbulent buoyancy flux b, both averaged over one oscillation period. The velocity profile shows an exchange flow with up–slope velocity near the bottom and down–slope velocity above. The location of the change in sign of velocity coincides exactly with the minimum of the turbulent buoyancy flux and is consistent with u being proportional to $-\partial b/\partial z$.

The mixing analysis by Klingbeil et al. (2014) and relation (9c) further render it possible to distinguish between the physically and numerically induced diahaline exchange flow. Despite the advanced numerical techniques of our coastal ocean model to reduce numerical mixing, the exchange flow across the majority of isohalines is associated up to 50% and more with numerical mixing. The maps of numerically induced, spurious diahaline salinity variance dissipation presented in this work, based on a column-by-column application of the water mass transformation framework, add to earlier methods developed for diathermal fluxes in Holmes et al. (2021, their Fig. 3).

Finally, this diahaline framework calls for its extension to the thermohaline overturning circulation of the World Ocean. Quantifying the contribution of the spurious numerically driven global circulation is of great interest for estimating the reliability of climate models.

Open Research Section

The model data used in this work are available from `https://doi.org/10.5281/zenodo.7754399` (Klingbeil, 2023).

References

Bergström, S., & Carlsson, B.   (1994).   River runoff to the Baltic Sea - 1950-1990. *Ambio*, *23*(4-5), 280–287.

Burchard, H.   (2020).   A Universal Law of Estuarine Mixing.   *J. Phys. Oceanogr.*, *50*(1), 81–93. doi: 10.1175/JPO-D-19-0014.1

Burchard, H., & Bolding, K. (2002). *GETM – a General Estuarine Transport Model. Scientific Documentation* (Tech. Rep. Nos. EUR 20253 EN, JRC23237).   European Commission.   Retrieved from `http://publications.jrc.ec.europa.eu/repository/handle/JRC23237`

Burchard, H., Bolding, K., Feistel, R., Gräwe, U., Klingbeil, K., MacCready, P., . . .

van der Lee, E. M. (2018). The knudsen theorem and the total exchange flow analysis framework applied to the baltic sea. *Progress in Oceanography*, *165*, 268-286. doi: https://doi.org/10.1016/j.pocean.2018.04.004

Burchard, H., Lange, X., Klingbeil, K., & MacCready, P. (2019). Mixing Estimates for Estuaries. *J. Phys. Oceanogr.*, *49*(2), 631–648. doi: 10.1175/JPO-D-18-0147.1

Burchard, H., & Rennau, H. (2008). Comparative quantification of physically and numerically induced mixing in ocean models. *Ocean Model.*, *20*(3), 293–311. doi: 10.1016/j.ocemod.2007.10.003

Chen, S.-N., Geyer, W. R., Ralston, D. K., & Lerczak, J. A. (2012). Estuarine exchange flow quantified with isohaline coordinates: Contrasting long and short estuaries. *Journal of Physical Oceanography*, *42*(5), 748 - 763. doi: 10.1175/JPO-D-11-086.1

Döös, K., Meier, H. E. M., & Döscher, R. (2004). The Baltic Haline Conveyor Belt or The Overturning Circulation and Mixing in the Baltic. *Ambio*, *33*(4), 261–266. doi: 10.1579/0044-7447-33.4.261

Döös, K., Nilsson, J., Nycander, J., Brodeau, L., & Ballarotta, M. (2012). The World Ocean Thermohaline Circulation. *J. Phys. Oceanogr.*, *42*(9), 1445–1460. doi: 10.1175/JPO-D-11-0163.1

Döös, K., & Webb, D. J. (1994). The Deacon Cell and the Other Meridional Cells of the Southern Ocean. *J. Phys. Oceanogr.*, *24*(2), 429–442. doi: 10.1175/1520-0485(1994)024⟨0429:TDCATO⟩2.0.CO;2

Feistel, R., Günther, N., & Eberhard, H. (2006). Unusual Baltic inflow activity in 2002-2003 and varying deep-water properties. *Oceanologia*, *48*(S).

Feistel, R., Günther, N., Wolfgang, M., & Eberhard, H. (2003). Temporal and spatial evolution of the Baltic deep water renewal in spring 2003. *Oceanologia*, *45*(4).

Feistel, R., Nausch, G., Mohrholz, V., Łysiak-Pastuszak, E., & Hansen, I. S. (2003). Warm waters of summer 2002 in the deep Baltic Proper. *Oceanologia*.

Ferrari, R., Mashayek, A., McDougall, T. J., Nikurashin, M., & Campin, J.-M. (2016). Turning ocean mixing upside down. *Journal of Physical Oceanography*, *46*(7), 2239 - 2261. doi: 10.1175/JPO-D-15-0244.1

Franck, H., Matthäus, W., & Sammler, R. (1987). Major inflows of saline water into the baltic sea during the present century. *Gerlands Beitr. Geophys.*, *96*, 517–531.

Garrett, C. (1990). The role of secondary circulation in boundary mixing. *Journal of Geophysical Research: Oceans*, *95*(C3), 3181-3188. doi: https://doi.org/10.1029/JC095iC03p03181

Gräwe, U., Flöser, G., Gerkema, T., Duran-Matute, M., Badewien, T. H., Schulz, E., & Burchard, H. (2016). A numerical model for the entire Wadden Sea: Skill assessment and analysis of hydrodynamics. *J. Geophys. Res. Oceans*, *121*(7), 5231–5251. doi: 10.1002/2016JC011655

Gräwe, U., Holtermann, P. L., Klingbeil, K., & Burchard, H. (2015). Advantages of vertically adaptive coordinates in numerical models of stratified shelf seas. *Ocean Modelling*, *92*, 56–68. doi: 10.1016/j.ocemod.2015.05.008

Gräwe, U., Klingbeil, K., Kelln, J., & Dangendorf, S. (2019). Decomposing mean sea level rise in a semi-enclosed basin, the Baltic Sea. *Journal of Climate*, *32*, 3089–3108. doi: 10.1175/JCLI-D-18-0174.1

Groeskamp, S., Griffies, S. M., Iudicone, D., Marsh, R., & Zika, J. D. (2019). The Water Mass Transformation Framework for Ocean Physics and Biogeochemistry. *Annu. Rev. Mar. Sci.*, *11*(1). doi: 10.1146/annurev-marine-010318-095421

Groeskamp, S., Zika, J. D., McDougall, T. J., Sloyan, B. M., & Laliberté, F. (2014). The Representation of Ocean Circulation and Variability in Thermodynamic Coordinates. *J. Phys. Oceanogr.*, *44*(7), 1735–1750. doi:

10.1175/JPO-D-13-0213.1

Hela, I. (1944). Über die Schwankungen des Wasserstandes in der Ostsee mit besonderer Berücksichtigung des Wasseraustausches durch die dänischen Gewässer. *undefined*.

Hetland, R. D. (2005). Relating river plume structure to vertical mixing. *J. Phys. Oceanogr.*, *35*(9), 1667–1688. doi: 10.1175/JPO2774.1

Hofmeister, R., Burchard, H., & Beckers, J.-M. (2010). Non-uniform adaptive vertical grids for 3d numerical ocean models. *Ocean Modelling*, *33*(1), 70-86. doi: https://doi.org/10.1016/j.ocemod.2009.12.003

Holmes, R. M., Zika, J. D., Griffies, S. M., Hogg, A. M., Kiss, A. E., & England, M. H. (2021). The Geography of Numerical Mixing in a Suite of Global Ocean Models. *Journal of Advances in Modeling Earth Systems*, *13*(e2020MS002333). doi: 10.1029/2020MS002333

Holtermann, P. L., Burchard, H., Gräwe, U., Klingbeil, K., & Umlauf, L. (2014). Deep-water dynamics and boundary mixing in a nontidal stratified basin: A modeling study of the baltic sea. *Journal of Geophysical Research: Oceans*, *119*(2), 1465-1487. doi: https://doi.org/10.1002/2013JC009483

Holtermann, P. L., & Umlauf, L. (2012). The baltic sea tracer release experiment: 2. mixing processes. *Journal of Geophysical Research: Oceans*, *117*(C1). doi: https://doi.org/10.1029/2011JC007445

Holtermann, P. L., Umlauf, L., Tanhua, T., Schmale, O., Rehder, G., & Waniek, J. J. (2012). The baltic sea tracer release experiment: 1. mixing rates. *Journal of Geophysical Research: Oceans*, *117*(C1). doi: https://doi.org/10.1029/2011JC007439

Klingbeil, K. (2023). *DiahalineBaltic GETM model results.* Zenodo [data set]. doi: 10.5281/zenodo.7754399

Klingbeil, K., & Burchard, H. (2013). Implementation of a direct nonhydrostatic pressure gradient discretisation into a layered ocean model. *Ocean Modelling*, *65*, 64–77. doi: 10.1016/j.ocemod.2013.02.002

Klingbeil, K., & Henell, E. (2023). A rigorous derivation of the water mass transformation framework, the relation between mixing and diasurface exchange flow, and links to recent theories in estuarine research. *Journal of Physical Oceanography.* doi: 10.1175/JPO-D-23-0130.1

Klingbeil, K., Lemarié, F., Debreu, L., & Burchard, H. (2018). The numerics of hydrostatic structured-grid coastal ocean models: state of the art and future perspectives. *Ocean Modelling*, *125*, 80–105. doi: 10.1016/j.ocemod.2018.01.007

Klingbeil, K., Mohammadi-Aragh, M., Gräwe, U., & Burchard, H. (2014). Quantification of spurious dissipation and mixing – Discrete Variance Decay in a Finite-Volume framework. *Ocean Model.*, *81*. doi: 10.1016/j.ocemod.2014.06.001

Knudsen, M. (1900). Ein hydrographischer lehrsatz. *Ann. Hydrogr. Marit. Meteor.*, *28*, 316–320.

Lee, M.-M., Coward, A. C., & Nurser, A. J. G. (2002). Spurious diapycnal mixing of the deep waters in an eddy-permitting global ocean model. *Journal of Physical Oceanography*, *32*(5), 1522 - 1535. doi: 10.1175/1520-0485(2002)032⟨1522: SDMOTD⟩2.0.CO;2

Lehmann, A., Myrberg, K., Post, P., Chubarenko, I., Dailidiene, I., Hinrichsen, H.-H., ... Bukanova, T. (2022). Salinity dynamics of the baltic sea. *Earth System Dynamics*, *13*(1), 373–392. doi: 10.5194/esd-13-373-2022

Li, X., Lorenz, M., Klingbeil, K., Chrysagi, E., Gräwe, U., Wu, J., & Burchard, H. (2022). Salinity mixing and diahaline exchange flow in a large multi-outlet estuary with islands. *Journal of Physical Oceanography*, *52*(9), 2111 - 2127. doi: 10.1175/JPO-D-21-0292.1

Liblik, T., & Lips, U. (2019). Stratification Has Strengthened in the Baltic Sea -An Analysis of 35 Years of Observational Data. *Frontiers of Earth Science*, *7*. doi:

10.3389/feart.2019.00174

MacCready, P. (2011). Calculating estuarine exchange flow using isohaline coordinates. *Journal of Physical Oceanography*, *41*(6), 1116 - 1124. doi: 10.1175/2011JPO4517.1

MacCready, P., Geyer, W., & Burchard, H. (2018). Estuarine exchange flow is related to mixing through the salinity variance budget. *Journal of Physical Oceanography*, *48*. doi: 10.1175/JPO-D-17-0266.1

MacCready, P., & Geyer, W. R. (2001). Estuarine salt flux through an isohaline surface. *Journal of Geophysical Research: Oceans*, *106*(C6), 11629–11637.

MacCready, P., Hetland, R., & Geyer, W. (2002). Long-term isohaline salt balance in an estuary. *Continental Shelf Research*, *22*, 1591-1601. doi: 10.1016/S0278-4343(02)00023-7

Matthäus, W. (2006). The history of investigation of salt water inflows into the Baltic Sea - from the early beginning to recent results. *Meereswissenschaftliche Berichte*, *65*. doi: 10.12754/msr-2006-0065

Megann, A. (2018). Estimating the numerical diapycnal mixing in an eddy-permitting ocean model. *Ocean Modelling*, *121*, 19-33. doi: https://doi.org/10.1016/j.ocemod.2017.11.001

Mohrholz, V., Dutz, J., & Kraus, G. (2006). The impact of exceptionally warm summer inflow events on the environmental conditions in the Bornholm Basin. *J. Mar. Syst.*, *60*(3-4), 285–301. doi: 10.1016/j.jmarsys.2005.10.002

Mohrholz, V., Naumann, M., Nausch, G., Krüger, S., & Gräwe, U. (2015). Fresh oxygen for the Baltic Sea — An exceptional saline inflow after a decade of stagnation. *J. Mar. Syst.*, *148*, 152–166. doi: 10.1016/j.jmarsys.2015.03.005

Purkiani, K., Becherer, J., Klingbeil, K., & Burchard, H. (2016). Wind-induced variability of estuarine circulation in a tidally energetic inlet with curvature. *Journal of Geophysical Research: Oceans*, *121*(5), 3261-3277. doi: https://doi.org/10.1002/2015JC010945

Reese, L., Gräwe, U., Klingbeil, K., Li, X., Lorenz, M., & Burchard, H. (2023). Local mixing determines spatial structure of diahaline exchange flow in a mesotidal estuary – a study of extreme runoff conditions. *Journal of Physical Oceanography*. doi: 10.1175/JPO-D-23-0052.1

Reissmann, J. H., Burchard, H., Feistel, R., Hagen, E., & Wieczorek, G. (2009). Vertical mixing in the Baltic Sea and consequences for eutrophication – A review. *Progress in Oceanography - PROG OCEANOGR*, *82*(1), 47–80. doi: 10.1016/j.pocean.2007.10.004

Sidorenko, D., Danilov, S., Fofonova, V., Cabos, W., Koldunov, N., Scholz, P., . . . Wang, Q. (2020). Amoc, water mass transformations, and their responses to changing resolution in the finite-volume sea ice-ocean model. *Journal of Advances in Modeling Earth Systems*, *12*(12), e2020MS002317. doi: https://doi.org/10.1029/2020MS002317

Sutherland, D. A., MacCready, P., Banas, N. S., & Smedstad, L. F. (2011). A model study of the Salish Sea estuarine circulation. *Journal of Physical Oceanography*, *41*(6), 1125–1143.

Umlauf, L., & Burchard, H. (2005). Second-order turbulence closure models for geophysical boundary layers. a review of recent work. *Continental Shelf Research*, *25*(7), 795-827. (Recent Developments in Physical Oceanographic Modelling: Part II) doi: https://doi.org/10.1016/j.csr.2004.08.004

Umlauf, L., & Burchard, H. (2011). Diapycnal transport and mixing efficiency in stratified boundary layers near sloping topography. *Journal of Physical Oceanography*, *41*(2), 329–345.

Walin, G. (1977). A theoretical framework for the description of estuaries. *Tellus*, *29*(2), 128–136. doi: 10.3402/tellusa.v29i2.11337

Walin, G. (1982). On the relation between sea-surface heat flow and thermal circulation in the ocean. *Tellus*, *34*(2), 187–195. doi: 10.1111/j.2153-3490.1982

.tb01806.x

Wang, T., Geyer, W. R., & MacCready, P. (2017). Total exchange flow, entrainment, and diffusive salt flux in estuaries. *Journal of Physical Oceanography*, *47*(5), 1205 - 1220. doi: 10.1175/JPO-D-16-0258.1

Wyrtki, K. (1954). Der große Salzeinbruch in die Ostsee im November und Dezember 1951. *Institut für Meereskunde*.

Zika, J. D., England, M. H., & Sijp, W. P. (2012). The Ocean Circulation in Thermohaline Coordinates. *J. Phys. Oceanogr.*, *42*(5), 708–724. doi: 10.1175/JPO-D-11-0139.1